# Whole Heart and Great Vessel Segmentation in Congenital Heart Disease Using Deep Neural Networks and Graph Matching

Xiaowei Xu[1(✉)], Tianchen Wang[1], Yiyu Shi[1], Haiyun Yuan[2], Qianjun Jia[2], Meiping Huang[2], and Jian Zhuang[2]

[1] University of Notre Dame, Notre Dame, USA
{xxu8,twang9,yshi4}@nd.edu
[2] Guangdong General Hospital, Guangzhou, China
yhyyun@163.com, jiaqianjun@126.com, huangmeipng@126.com, zhuangjian5413@tom.com

**Abstract.** Congenital heart disease (CHD) is the leading cause of mortality from birth defects, which occurs 1 in every 110 births in the United States. While various whole heart and great vessel segmentation frameworks have been developed in the literature, they are ineffective when applied to medical images in CHD, which have significant variations in heart structure and great vessel connections. To address the challenge, we leverage the power of deep learning in processing regular structures and that of graph algorithms in dealing with large variations, and propose a framework that combines both for whole heart and great vessel segmentation in CHD. Particularly, we first use deep learning to segment the four chambers and myocardium followed by blood pool, where variations are usually small. We then extract the connection information and apply graph matching to determine the categories of all the vessels. Experimental results using 68 3D CT images covering 14 types of CHD show that our method can increase Dice score by 12% on average compared with the state-of-the-art whole heart and great vessel segmentation method in normal anatomy. Our dataset is released to the public.

**Keywords:** Congenital heart disease · Segmentation · Deep neural networks · Graph matching

## 1 Introduction

Congenital heart disease (CHD) is the most common cause of infant death due to birth defects [3]. It usually comes with significant variations in heart structures and great vessel connections, which renders general whole heart and great vessel segmentation methods [9,11] in normal anatomy ineffective. Most existing segmentation methods dedicated to CHD target blood pool and myocardium only


D. Shen et al. (Eds.): MICCAI 2019, LNCS 11765, pp. 477–485, 2019.
https://doi.org/10.1007/978-3-030-32245-8_53

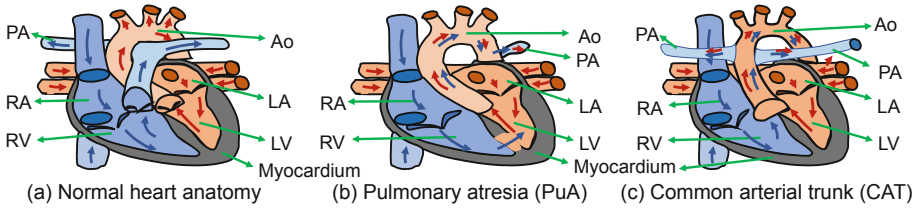


**Fig. 1.** Examples of large structure variations in CHD. In normal heart anatomy (a), PA is connected to RV. However, in pulmonary atresia (b), PA is rather small and connected to descending Ao. In common arterial trunk (c), Ao is connected to both RV and LV, and PA is connected to Ao.

[13,16]. Recently, semi-automated segmentation in CHD has also been explored [8], which requires users to locate an initial seed. However, fully automated segmentation of whole heart and great vessel segmentation in CHD still remains a missing piece in the literature.

Inspired by the success of graph matching in a number of applications with large variations [4], in this paper we propose to combine deep learning [6,7,12, 14,15] and graph matching for fully automated whole heart and great vessel segmentation in CHD. Particularly, we leverage deep learning to segment the four chambers and myocardium followed by blood pool, where variations are usually small and accuracy can be high. We then extract the vessel connection information and apply graph matching to determine the categories of all the vessels. Compared with the state-of-the-art method for whole heart and great vessel segmentation in normal anatomy, our method can achieve 12% higher Dice score. Our dataset including 68 3D CT images with 14 types of CHD is available at [1].

## 2 Background

Within normal heart anatomy as shown in Fig. 1(a), there are usually seven substructures: left ventricle (LV), right ventricle (RV), left atrium (LA), right atrium (RA), myocardium (Myo), faorta (Ao) and pulmonary artery (PA). Note that the area including RA, LA, LV, RV, PA, and Ao is defined as blood pool. However, CHD usually suffers from significant variations in heart structure and great vessel connections. Six common types of CHD [3] include: atrial septal defect (ASD), atrio-ventricular septal defect (AVSD), patent ductus arteriosus (PDA), pulmonary stenosis (PS), ventricular septal defect (VSD), co-arctation (CA). Figure 1(b) and (c) shows two less common types with larger variations, where we can notice that PA is connected to Ao rather than RV. As existing methods perform pixel-wise classification based on the surrounding pixels in the receptive field, the disappeared main trunk of PA renders them ineffective.

**Table 1.** The types of CHD in our dataset and the associated number of images. Note that some images may correspond to more than one type of CHD.

| Common CHD | | | | | | Less common CHD | | | | | | | | Normal |
|---|---|---|---|---|---|---|---|---|---|---|---|---|---|---|
| ASD | AVSD | VSD | PDA | CA | PS | ToF | TGA | PAS | AD | CAT | AAA | SV | PuA | |
| 17 | 4 | 26 | 7 | 4 | 4 | 7 | 4 | 3 | 20 | 4 | 8 | 2 | 7 | 2 |

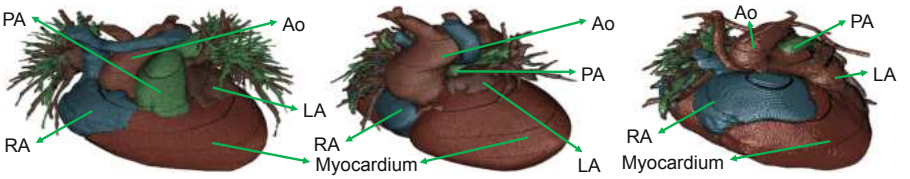


(a) Normal heart anatomy (b) Pulmonary atresia (PuA) (c) Common arterial trunk (CAT)

**Fig. 2.** Pulmonary atresia and common arterial trunk examples in our dataset, with large variations from normal heart anatomy.

## 3 Dataset

Our dataset consists of 68 3D CT images captured by a Simens biograph 64 machine. The ages of the associated patients range from 1 month to 21 years, with majority between 1 month and 2 years. The size of the images is $512 \times 512 \times (130 - 340)$, and the typical voxel size is $0.25 \times 0.25 \times 0.5\,\text{mm}^3$. The dataset covers 14 types of CHD, which include the six common types discussed in Sect. 2 plus eight less common ones (Tetrology of Fallot (ToF), transposition of great arteries (TGA), pulmonary artery sling (PAS), anomalous drainage (AD), common arterial trunk (CAT), aortic arch anomalies (AAA), single ventricle (SV), pulmonary atresia (PuA)). The number of images associated with each is summarized in Table 1. All labeling were performed by experienced radiologists, and the time for labeling each image is 1–1.5 h. The labels include seven substructures: LV, RV, LA, RA, Myo, Ao and PA. For easy processing, venae cavae (VC) and pulmonary vein (PV) are also labeled as part of RA and LA respectively, as they are connected and their boundaries are relatively hard to define. Anomalous vessels are also labeled as one of the above seven substructures based on their connections. Figure 2 shows 3D views of some examples in our dataset with significant structure variations.

## 4 Method

**Overview**: The overall framework is shown in Fig. 3. **Region of interest (RoI) cropping** extracts the area that includes the heart and its surrounding vessels. We resize the input image to a low resolution of $64 \times 64 \times 64$, and then adopt the same segmentation-based extraction as [9] to get the RoI. **Chambers and myocardium segmentation** resizes the extracted RoI to $64 \times 64 \times 64$ which

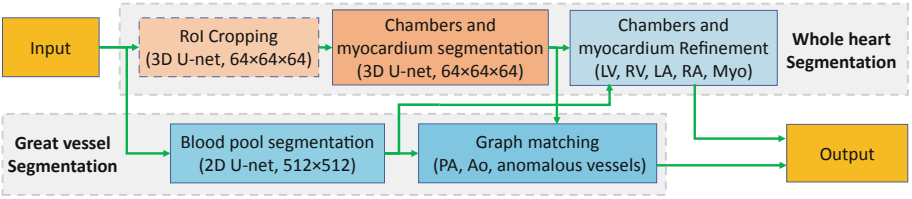


**Fig. 3.** Overview of the proposed framework combining deep learning and graph matching for whole heart and great vessel segmentation in CHD.

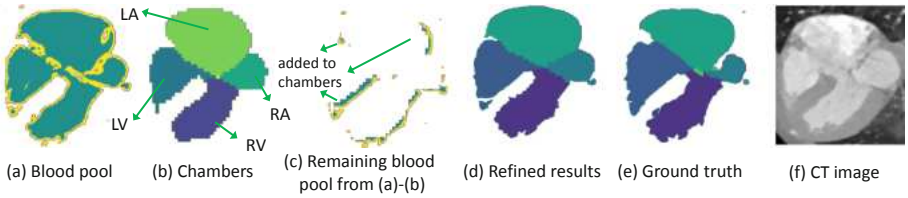


**Fig. 4.** Illustration of chambers and myocardium refinement. (a) is obtained from blood pool segmentation (high resolution). (b) is from chambers and myocardium segmentation (low resolution). (c) is the remaining blood pool by subtracting chambers (b) from blood pool (a). It is added to the surrounding chambers to refine the boundaries (d). (e) and (f) are the ground truth and CT image, respectively.

is fed to a 3D U-net for segmentation. **Blood pool segmentation** is conducted on each 2D slice of the input using a 2D U-net [10] with an input size of $512 \times 512$. Note that in order to detect the blood pool boundary for easy graph extraction in graph matching later, we add another class blood pool boundary in the segmentation. **Chambers and myocardium refinement** refines the boundaries of chambers and myocardium based on the outputs of chambers and myocardium segmentation and blood pool segmentation. **Graph matching** identifies Ao, PA and anomalous vessels using the outputs of blood pool segmentation and chambers and myocardium segmentation. More details about chambers and myocardium refinement and graph matching are discussed as follows.

**Chambers and Myocardium Refinement**: To avoid excessive memory consumption and over-fitting [9], the input of 3D U-net is usually limited to low resolution or small size, and accordingly the chambers and myocardium segmentation results may lose boundary information. This is critical for CHD where significant variations exist. To address this issue, we refine the boundary of chambers and myocardium by reusing the blood pool segmentation results, which is in high resolution. Specifically, we remove the portion of blood pool that corresponds to the chambers from the results of blood pool segmentation, and the remaining blood pool is added to its surrounding chambers to refine the boundaries. With the refined boundary of chambers, the boundary of myocardium is also refined as the chambers and the myocardium share a large portion of boundaries as shown

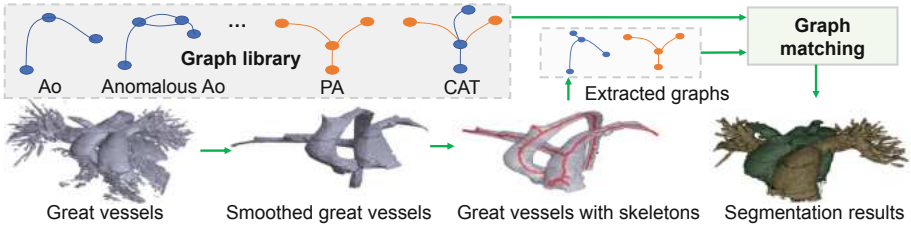


**Fig. 5.** Illustration of great vessel segmentation with graph matching. With smoothing, the skeleton of great vessels can be easily extracted, and then its corresponding graph is obtained for graph matching based classification of Ao, PA and anomalous vessels.

in Fig. 1. An illustration of the refinement process is shown in Fig. 4. Comparing (b) with (e), we can notice that part of the boundary information is lost, and the boundary is indeed refined after the process as shown in (d).

**Graph Matching**: Great vessels can be obtained by removing the chambers areas from the blood pool, which need to be segmented to identify Ao, PA as well as anomalous vessels. This is where significant variations can occur in CHD. To address this issue, we adopt a surface thinning algorithm [5] to obtain skeletons of blood vessels for graph matching, and the workflow is shown in Fig. 5. A graph library is built to represent all the possible connections of great vessels and anomalous vessels. We then extract the graphs corresponding to Ao, PA, and anomalous vessels or their mixtures. Note that these extracted graphs should be disconnected from each other to match with the ones in the library. However, due to inaccurate blood pool segmentation or small anomalous connections, the graphs are often fused together, making the matching difficult. To tackle this issue, we apply multiple smoothing in various scales to extract several candidate graphs. Then we match these graphs with the ones in the library to identify the most similar pairs. With graph matching, the categories of the extracted graphs as well as the categories of the corresponding vessels in these graphs can be determined (based on the labeled graphs in the library). The vessels that are left out in the smoothing process are finally classified by a simple region growing technique [2].

## 5 Experiments

**Experiment Setup**: All the experiments run on a Nvidia GTX 1080Ti GPU with 11 GB memory. We implement our 3D U-net using Pytorch based on [9]. For 2D U-net, most configurations remain the same with those of the 3D U-net except that 2D U-net adopts 5 levels and the number of filters in the initial level is 16. Both Dice loss and cross entropy loss are used, and the training epochs are 6 and 480 for 2D U-net and 3D U-net, respectively. Data augmentation is also adopted with the same configuration as in [9] for 3D U-net. Data normalization is the same as [9]. The learning rate is 0.0002 for the first 50% epochs, and

**Table 2.** Mean and standard deviation of Dice score of the state-of-the-art method Seg-CNN [9] and our method (in %) for seven substructures of whole heart and great vessel segmentation.

| Method | LV | RV | LA | RA | Myo | Ao | PA | Average |
|---|---|---|---|---|---|---|---|---|
| Seg-CNN [9] | 67.3 | 65.0 | 70.2 | 76.0 | 71.5 | 63.0 | 52.3 | 66.5 |
| std | ±13.9 | ±12.0 | ±7.8 | ±7.5 | ±8.3 | ±13.3 | ±12.3 | ±10.7 |
| Our method | 82.4 | 77.6 | 78.6 | 82.7 | 77.3 | 82.2 | 67.1 | 78.3 |
| std | ±10.5 | ±14.3 | ±7.4 | ±7.5 | ±8.3 | ±8.1 | ±19.8 | ±10.8 |

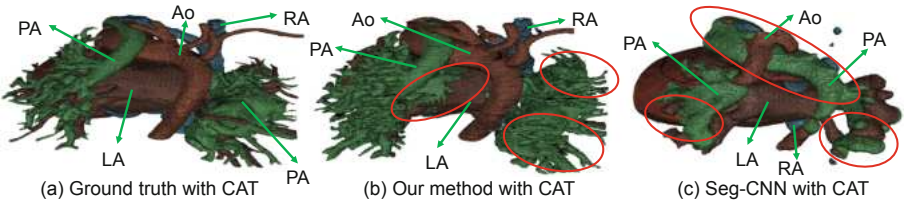


**Fig. 6.** Visualized comparison between the state-of-the-art method Seg-CNN [9] and our method. The differences from the ground truth are highlighted by the red circles. (Color figure online)

**Table 3.** Mean and standard deviation of Dice score of the state-of-the-art method Seg-CNN [9] and our method (in %) in mild and severe CHDs.

| Method | Mild CHD (VSD, ASD, AVSD, PDA) | Severe CHD (others) |
|---|---|---|
| Seg-CNN [9] | $70.3 \pm 8.3$ | $62.7 \pm 14.4$ |
| Our method | $82.6 \pm 6.2$ | $74.1 \pm 14.5$ |

then 0.00002 afterward. We adopt Seg-CNN [9] that achieves the state-of-the-art performance in whole heart and great vessel segmentation within normal anatomy for comparison. The configuration is the same as that in [9].

For both methods, four-fold cross validation is performed (17 images for testing and 51 images for training). The split of our dataset considers the structures of CHD so that any structure in the testing dataset also has a similar presence in the training dataset, though they may be not of the same type of CHD. The Dice score is used for segmentation evaluation.

**Results and Analysis**: The comparison with Seg-CNN [9] is shown in Table 2. Our method can get 5.8%–19.2% higher mean Dice score across the seven substructures (12% higher on average). The highest improvement is achieved in Ao, which is due to its simple graph connection with successful graph matching. The least improvement is obtained in myocardium, which is due to the fact that myocardium is not well considered in the high-resolution blood pool segmentation. Visualization of CAT segmentation using our method and Seg-CNN is

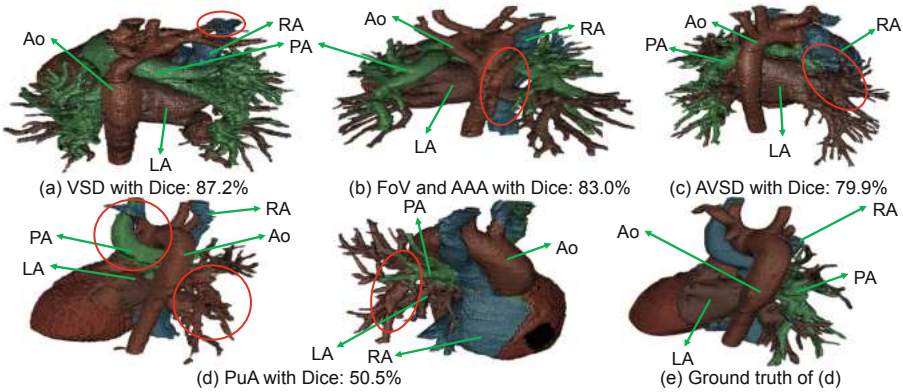


**Fig. 7.** Visualization of our segmentation results with (a) best, (b)(c) median, and (d) worst Dice scores among all the test images. The ground truth of (d) is shown in (e). Red circles indicate the segmentation error. (Color figure online)

shown in Fig. 6. Our method can clearly segment Ao and PA with some slight mis-segmentation between PA and LA. However, Seg-CNN segments the main part of Ao as PA, which is due to the fact that pixel-level segmentation by U-net is only based on the surrounding pixels, and the connection information is not well exploited.

The segmentation performance of our method and Seg-CNN [9] in different scenarios (mild and severe CHDs) [3] is shown in Table 3. Both methods achieve higher mean Dice with lower standard deviations in mild CHD than in severe CHD, as severe CHD has more complicated structure variations. Compared with Seg-CNN, our method can achieve about 12% higher mean Dice score on both mild and severe CHDs on average. Our method also achieves a 1.9% reduction on standard deviation of Dice score in mild CHD compared with Seg-CNN [9].

Finally, visualizations of segmentation results from our method with best, median and worst Dice score among all the test images are shown in Fig. 7. The segmentation result in Fig. 7(a) achieves the best accuracy, and most of the structures are segmented correctly, with some error in the tiny connections between RA and Ao as indicated by the red circle. The segmentation results in Fig. 7(b) and (c) have some more serious mis-segmentation: the one in Fig. 7(b) has an anomalous vein from RA which is segmented as part of Ao due to the boundary extraction error in blood pool segmentation, and the one in Fig. 7(c) suffers from the boundary extraction error between LA and PA. This type of error also leads to the result with the worst Dice score as shown in Fig. 7(d), with corresponding ground truth provided in (e). In the ground truth, a thick anomalous vein from RA crosses Ao, and PA has no trunk vessels and is of a very small volume. Compared with the ground truth, the thick anomalous vein from RA is mis-classified as PA, and the majority of PA is mis-classified as LA. In the future work, we will try to solve this problem to correctly extract all the critical boundaries.

## 6 Conclusion

In this paper we proposed a whole heart and great vessel segmentation framework for CT images in CHD. We first used deep learning to segment the four chambers and myocardium followed by blood pool, where variations are usually small. We then extracted the connection information and apply graph matching to determine the categories of all the vessels. We collected a CHD dataset in CT with 68 3D images, and the ground truth has seven categories: LV, RV, LA, RA, myocardium, Ao and PA. Totally 14 types of CHD are included in this dataset which is made publicly available. Compared with the state-of-the-art method for whole heart and great vessel segmentation in normal anatomy, our method can achieve 12% improvement in Dice score on average.

**Acknowledgement.** This work was approved by the Research Ethics Committee of Guangdong General Hospital, Gunagdong Academy of Medical Sciences with protocol No. 20140316. This work was supported by the National key Research and Development Program [2018YFC1002600], Science and Technology Planning Project of Guangdong Province, China [No. 2017A070701013, 2017B090904034, 2017030314 109, and 2019B020230003], and Guangdong peak project [DFJH201802].

## References

1. Chd segmentation dataset. https://github.com/XiaoweiXu/Whole-heart-and-great-vessel-segmentation-of-chd_segmentation/tree/master
2. Adams, R., Bischof, L.: Seeded region growing. IEEE Trans. Pattern Anal. Mach. Intell. **16**(6), 641–647 (1994)
3. Bhat, V., BeLaVaL, V., Gadabanahalli, K., Raj, V., Shah, S.: Illustrated imaging essay on congenital heart diseases: multimodality approach part i: clinical perspective, anatomy and imaging techniques. J. Clin. Diagn. Res. JCDR **10**(5), TE01 (2016)
4. Lajevardi, S.M., Arakala, A., Davis, S.A., Horadam, K.J.: Retina verification system based on biometric graph matching. IEEE Trans. Image Process. **22**(9), 3625–3635 (2013)
5. Lee, T.C., Kashyap, R.L., Chu, C.N.: Building skeleton models via 3-d medial surface axis thinning algorithms. CVGIP Gr. Models Image Process. **56**(6), 462–478 (1994)
6. Li, B., Chenli, C., Xu, X., Jung, T., Shi, Y.: Exploiting computation power of blockchain for biomedical image segmentation. In: Proceedings of the IEEE Conference on Computer Vision and Pattern Recognition Workshops, pp. 0–0 (2019)
7. Liu, Z., et al.: Machine vision guided 3d medical image compression for efficient transmission and accurate segmentation in the clouds. arXiv preprint arXiv:1904.08487 (2019)
8. Pace, D.F., et al.: Iterative segmentation from limited training data: applications to congenital heart disease. In: Stoyanov, D., et al. (eds.) DLMIA/ML-CDS -2018. LNCS, vol. 11045, pp. 334–342. Springer, Cham (2018). https://doi.org/10.1007/978-3-030-00889-5_38

9. Payer, C., Štern, D., Bischof, H., Urschler, M.: Multi-label whole heart segmentation using0 CNNs and anatomical label configurations. In: Pop, M., et al. (eds.) STACOM 2017. LNCS, vol. 10663, pp. 190–198. Springer, Cham (2018). https://doi.org/10.1007/978-3-319-75541-0_20
10. Ronneberger, O., Fischer, P., Brox, T.: U-Net: convolutional networks for biomedical image segmentation. In: Navab, N., Hornegger, J., Wells, W.M., Frangi, A.F. (eds.) MICCAI 2015. LNCS, vol. 9351, pp. 234–241. Springer, Cham (2015). https://doi.org/10.1007/978-3-319-24574-4_28
11. Wang, C., MacGillivray, T., Macnaught, G., Yang, G., Newby, D.: A two-stage 3d unet framework for multi-class segmentation on full resolution image. arXiv preprint arXiv:1804.04341 (2018)
12. Wang, T., Xiong, J., Xu, X., Shi, Y.: Scnn: A general distribution based statistical convolutional neural network with application to video object detection. arXiv preprint arXiv:1903.07663 (2019)
13. Wolterink, J.M., Leiner, T., Viergever, M.A., Išgum, I.: Dilated convolutional neural networks for cardiovascular MR segmentation in congenital heart disease. In: Zuluaga, M.A., Bhatia, K., Kainz, B., Moghari, M.H., Pace, D.F. (eds.) RAMBO/HVSMR -2016. LNCS, vol. 10129, pp. 95–102. Springer, Cham (2017). https://doi.org/10.1007/978-3-319-52280-7_9
14. Xu, X., et al.: Quantization of fully convolutional networks for accurate biomedical image segmentation. In: Proceedings of the IEEE Conference on Computer Vision and Pattern Recognition, pp. 8300–8308 (2018)
15. Xu, X., et al.: Dac-sdc low power object detection challenge for uav applications. arXiv preprint arXiv:1809.00110 (2018)
16. Yu, L., Yang, X., Qin, J., Heng, P.-A.: 3D FractalNet: dense volumetric segmentation for cardiovascular MRI volumes. In: Zuluaga, M.A., Bhatia, K., Kainz, B., Moghari, M.H., Pace, D.F. (eds.) RAMBO/HVSMR -2016. LNCS, vol. 10129, pp. 103–110. Springer, Cham (2017). https://doi.org/10.1007/978-3-319-52280-7_10